RESEARCH ARTICLE
PLANETARY SCIENCES

Earth and Planetary Physics
7: 331–346, 2023
doi: 10.26464/epp2023005

Observations and interpretations of geomorphologic features in the Tianwen-1 landing area on Mars by using orbital imagery data

Hai Huang[1,2*], Xing Wang[1,2], Yuan Chen[1,2], Qing Zhang[1,2], FeiYue Zhao[1,2], Xin Ren[1], XingGuo Zeng[1], Wei Yan[1], WangLi Chen[1], Bin Liu[1], DaWei Liu[1], LianBo Fu[1,2], and JianJun Liu[1,2]

[1]Key Laboratory of Lunar and Deep Space Exploration, National Astronomical Observatories, Chinese Academy of Sciences, Beijing 100101, China;
[2]School of Astronomy and Space Science, University of Chinese Academy of Sciences, Beijing 100049, China

Key Points:

- A detailed geomorphologic map of the landing area has been constructed.
- Observed igneous-related features imply a subsurface heat source.
- Thermal and water ice-related influences affect the surface features.

Citation: Huang, H., Wang, X., Chen, Y., Zhang, Q., Zhao, F. Y., Ren, X., Zeng, X. G., Yan, W., Chen, W. L., Liu, B., Liu, D. W., Fu, L. B., and Liu, J. J. (2023). Observations and interpretations of geomorphologic features in the Tianwen-1 landing area on Mars by using orbital imagery data. *Earth Planet. Phys.*, *7*(3), 331–346. http://doi.org/10.26464/epp2023005

Abstract: China's first Mars exploration mission, Tianwen-1, successfully landed in southern Utopia Planitia on Mars on May 15, 2021. This work presents a detailed investigation of the geologic context of the landing area surface for this mission based on orbital remote-sensing data. We constructed a geomorphologic map for the Tianwen-1 landing area. Results of our detailed geomorphologic map show several major landforms within the landing area, including rampart craters, mesas, troughs, cones, and ridges. Analysis of materials on the landing area surface indicates that most of the landing area is covered by Martian dust. Transverse aeolian ridges are widely distributed within the landing area, indicating the surface contexts were (and still are) modified by regional winds. In addition, a crater counting analysis indicates the landing area has an absolute model age of ~3.3 Ga and that a later resurfacing event occurred at ~1.6 Ga. Finally, we outline four formational scenarios to test the formation mechanisms for the geomorphologic features on the landing area surface. The most likely interpretation to explain the existence of the observed surface features can be summarized as follows: A thermal influence may have played an important role in the formation of the surface geomorphologic features; thus, igneous-related processes may have occurred in the landing area. Water ice may also have been involved in the construction of the primordial surface configuration. Subsequent resurfacing events and aeolian processes buried and modified the primordial surface.

Keywords: Mars; Utopia Planitia; Tianwen-1; geomorphologic features; water ice; heat source

1. Introduction

China's first Mars exploration mission, Tianwen-1 (TW-1), which aims at completing orbiting, landing, and roving in one mission, was launched on July 23, 2020. As part of the TW-1 mission, the Zhurong rover landed at 109.925°E, 25.066°N on the surface of southern Utopia Planitia (Liu JJ et al., 2022). It is also the first rover to land in the southern Utopia Planitia of Mars. The orbiter and rover of this mission carried 13 scientific payloads (Li CL et al., 2021). These scientific payloads will be used to conduct global and local surveys during the TW-1 mission of the Martian climate and atmosphere, surface structures, water ice distribution, and surface material composition (Li CL et al., 2021). Meanwhile, a detailed local geologic investigation will be conducted in the landing area by using the instruments on the orbiter and rover.

Correspondence to: H. Huang, huangh@nao.cas.cn
Received 22 JUN 2022; Accepted 12 OCT 2022.
Accepted article online 28 OCT 2022.

The landing area of TW-1 is located in southern Utopia Planitia. The Utopia Planitia region of the Martian northern plains is known as an ancient circular impact basin centered at ~45°N, ~120°E with a diameter of 3,300 km (McGill, 1989; Thomson and Head, 2001). In many studies, several landforms within Utopia Planitia have been reported, such as giant polygons and polygonal terrain (Hiesinger and Head, 2000; Buczkowski et al., 2012), periglacial features (Soare et al., 2012), mud volcanoes (Skinner and Tanaka, 2007), and pancake and rampart craters (Ivanov et al., 2014). These records reflect the complex geologic evolutionary history of Utopia Planitia. In fact, the Utopia Planitia region has undergone various geologic processes, including volcanic, fluvial, glacial, and wind processes (Hiesinger and Head, 2000; Head et al., 2002; Soare et al., 2012; Tanaka et al., 2014; Costard et al., 2016). Head et al. (2002) described the bulk of the Martian northern lowlands as Early Hesperian-aged ridged plains of volcanic origin. Moreover, Lanz et al. (2010) first reported a small-scale volcanic rift zone in southwestern Utopia Planitia, and they proposed more widespread volcanic activity in the Late Noachian to Early Hesperian. These volcanic-related studies of Utopia Planitia indicate that

stable and active underground heat sources (e.g., magma chambers) may have existed in this region in the past. Periglacial features and ice-rich terrain are often present at midlatitudes (Soare et al., 2012, 2015), and the putative ancient ocean in the northern lowlands is another potentially important geologic setting of Utopia Planitia (Parker et al., 1993; Head et al., 1999). Previous studies suggest the possibility that water ice was present in the northern plains of Mars and Utopia Planitia (Parker et al., 1993; Head et al., 1999; Ivanov et al., 2014). Zuber et al. (2000) also considered the possibility that volcanic and sedimentary materials had infilled Utopia Planitia. It is interesting that very few actual traces of that volcanic-related activity in Utopia Planitia exist, and it is difficult to detect hydrous minerals or to find other direct evidence of water ice in Utopia Planitia through the orbital remote-sensing survey regardless of whether a large standing body of water (ocean hypothesis) ever occurred. In addition, the bulk of the northern hemisphere lowlands has undergone extensive resurfacing, especially the Vastitas Borealis Formation (VBF), which probably represents one of the final stages of water-related sedimentary activity that could have covered much of the northern plains during the Late Hesperian to Early Amazonian (Tanaka et al., 2003). Almost all the primordial ancient surface structures have been destroyed or buried. Aeolian processes are probably the dominant currently active surface-modifying processes on Mars (Greeley and Thompson, 2003).

Our study area is the TW-1 landing area (Figure 1a), which is located at the southern edge of Utopia Planitia and between the two Martian volcanic provinces of Elysium and Syrtis Major. The global geologic map of Mars (Tanaka et al., 2014) shows that the entire landing area is in a Late Hesperian lowland unit. Vastitas Borealis Formation materials covered this region. The high-resolution imaging camera (HiRIC) onboard the TW-1 orbiter provides complete imagery coverage of the study area. Recent publications have described much of the same ground (Mills et al., 2021; Wu B et al., 2021; Wu X et al., 2021; Ye BL et al., 2021; Zhao JN et al., 2021; Liu JJ et al., 2022). Wu B et al. (2021) conducted a survey mainly on the topographic characteristics (e.g., slope, rock abundance, etc.) of the TW-1 candidate landing region. Zhao JN et al. (2021) surveyed the stratigraphic relationships of the Zhurong landing site and proposed a five-layer stratigraphic model. In several studies, a comprehensive geological survey has been conducted of a large-scale region, and various landforms within this region have been discussed (Mills et al., 2021; Wu X et al., 2021; Ye BL et al., 2021). Our previous study provided the exact position of the Zhurong landing site and the scientific focus of the landing site (Liu JJ et al., 2022). In this work, we mainly use the HiRIC images to conduct a detailed examination and analysis of the surface features of the local landing region. We also discuss the formation and existence of the observed surface features.

2. Data and Methods

Our analyses are mainly based on a HiRIC digital orthophoto map (DOM) and a digital elevation model (DEM). Before the Zhurong rover touched down in southern Utopia Planitia, the TW-1 stereo camera on the charge-coupled device acquired enough HiRIC stereo images to fully cover the primary candidate landing area. These images were acquired at an orbital height of ~350 km with a spatial resolution of ~0.7 m (Liu JJ et al., 2022) and an imaging spectral range of 0.45–0.9 μm (Yan W et al., 2021). The DEM and DOM of the entire landing area were derived from these stereo images through a series of processing methods (Liu JJ et al., 2022). We examined the topographic and geomorphologic details of the

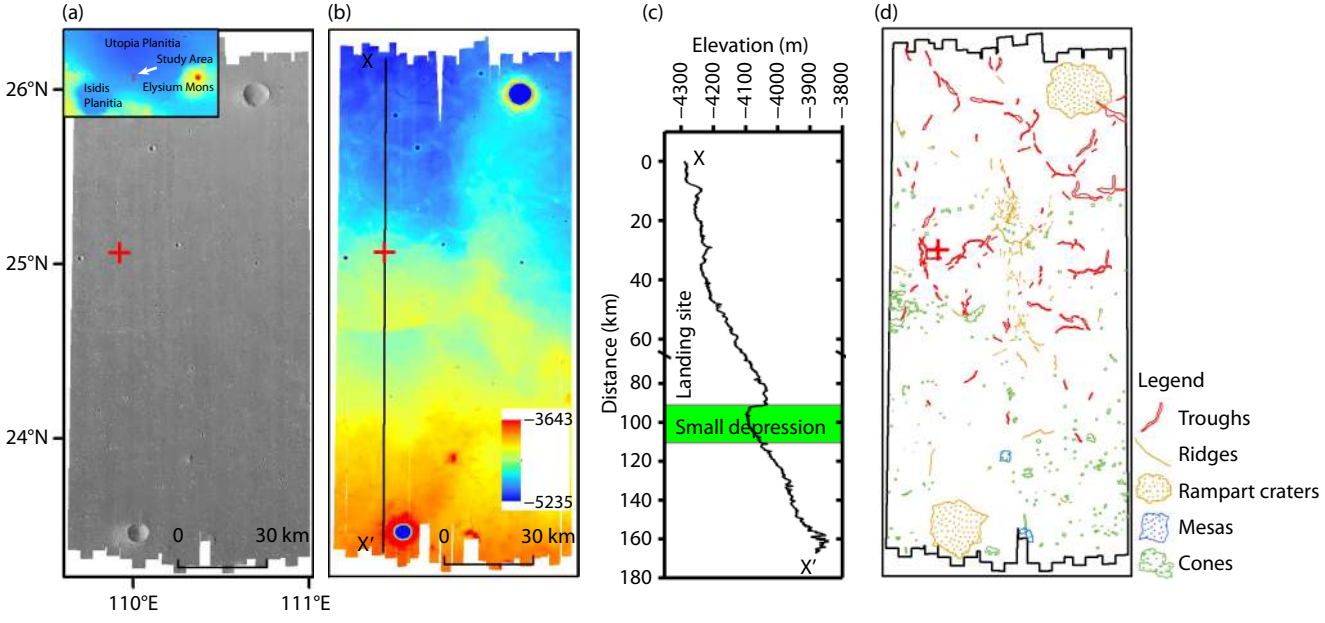

Figure 1. (a) Digital orthophoto map of the landing area derived from high-resolution imaging camera (HiRIC) images. The image in the top left corner indicates the position of the landing area in Utopia Planitia. The red cross indicates the Zhurong landing site. (b) Digital elevation model of the landing area derived from HiRIC stereo images. (c) The north–south topographic profile across the Zhurong landing site (X–X′ black line in panel b). The small depression is the outlined green area. (d) Geomorphologic map of the landing area. The red cross indicates the Zhurong landing site.

landing area by using the HiRIC-derived DOM (~0.7 m/pixel) and DEM (~3.5 m/pixel).

To acquire important information on the absolute model ages (AMAs) of the mapped units, crater size–frequency distribution (CSFD) measurements (Hartmann and Neukum, 2001) were performed with the HiRIC images. We derived AMAs by applying the production function of Ivanov (2001) and the chronology function of Neukum et al. (2001). CraterStats-II software (Michael and Neukum, 2010) was used in this study. Craters were measured and counted by using the CraterTools tool of the ArcMap software. Secondary craters (e.g., crater chains, crater clusters) were excluded from the crater counting, and 23,050 craters in the diameter range of 0.02–9.00 km were measured.

3. Observations and Analyses

The TW-1 landing area is located in the southern Utopia Planitia of Mars (Figure 1a). The southern landing area is topographically higher than the northern landing area, and a small depression appears in the landing area (Figures 1b and 1c). The main observed geomorphologic features in the landing area include ridges, rampart craters, mesas, cones, and troughs. The preliminary geomorphologic map shows the distribution of the identified features (Figure 1d). Three landforms (e.g., ridges, cones, and troughs) are relatively large in number, and the density map in Figure 2 indicates the main spatial distribution of these landforms.

3.1 Ridges

The observed ridges have a random spatial distribution (Figure 1d). In total, 161 ridges were identified, and most of them appear in the center of the landing area (Figure 2a). In our study area, the ridges range from 164 m to 12.8 km in length and a few meters in height. Many different geologic processes can produce ridge-like landforms on Mars, such as eskers and inverted stream beds. Periglacial features can be observed in the midlatitudes but not in the southern edge of Utopia Planitia. Thus, eskers can be excluded. Inverted stream beds are usually ridgelike features with flat upper surfaces; however, the ridges in our study area appear to have sharp crests. Structures resembling wrinkle ridges appear in the study area (Figures 3a and 3b), and the occurrence of wrinkle ridges in a smooth plain indicates that this plain has been rebuilt based on volcanic plains observed on Mars and other terrestrial planets (Solomon and Head, 1980; Chicarro et al., 1985; Bilotti and Suppe, 1999). The results of our observations agree well with those of an earlier study by Head et al. (2002), who proposed that the northern plains were formed by an Early Hesperian-aged volcanic ridged plain. It is interesting that some narrow, sharp-crested ridges (Figures 3c–3e, denoted by white arrows) up to ~100 m in basal width have a diminished topographic difference from the surrounding terrains. The linear ridges showing sharp crest characteristics are interpreted as eroded and exposed magmatic intrusions (dikes; Head et al., 2006; Korteniemi et al., 2010). As shown in Figure 3e, a dike crosscuts the cones, indicating the probability of proximal magmatic activity roughly at the time of cone and ridge formation. Lanz et al. (2010) compared dikes in their study area (a volcanic rift zone in southwestern Utopia Planitia) with dikes on Earth from Colorado, USA. We also compared dikes in our study area with dikes on Earth (Figure 3f) and observed the same sharp crest characteristics.

3.2 Rampart Craters

In Utopia Planitia, subsurface volatiles (e.g., water, ice, etc.) are an essential scientific focus. Some geomorphologic features have

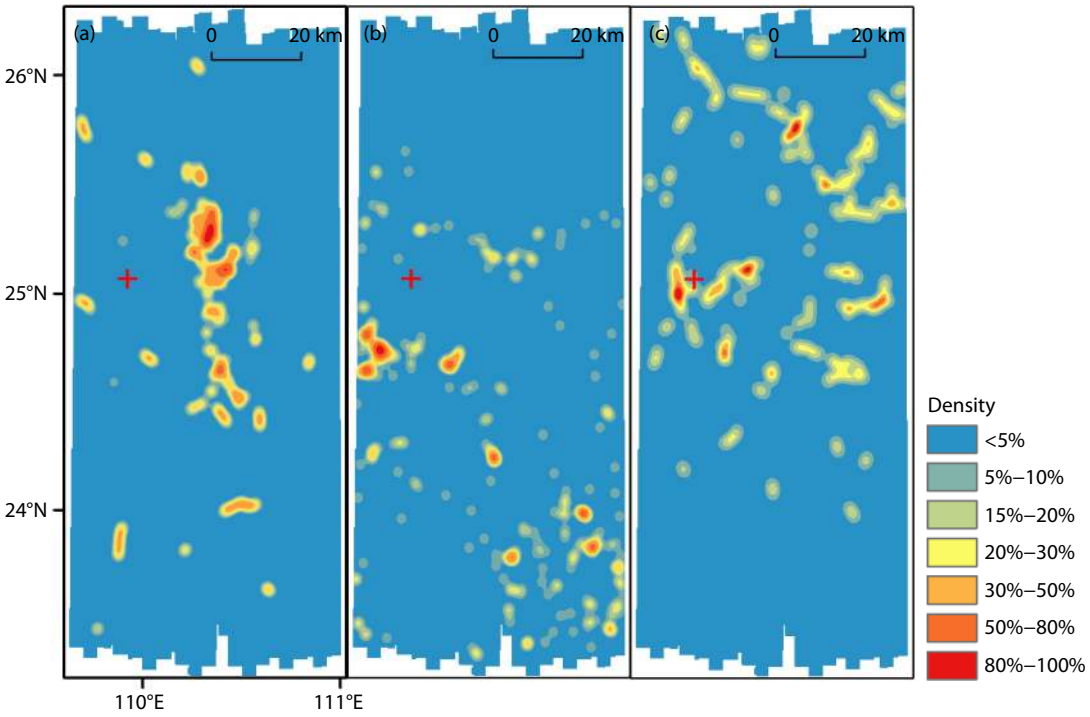

Figure 2. Density maps of (a) ridges, (b) cones and (c) troughs in the landing area. The red cross indicates the Zhurong landing site, and the search radius is 3 km.

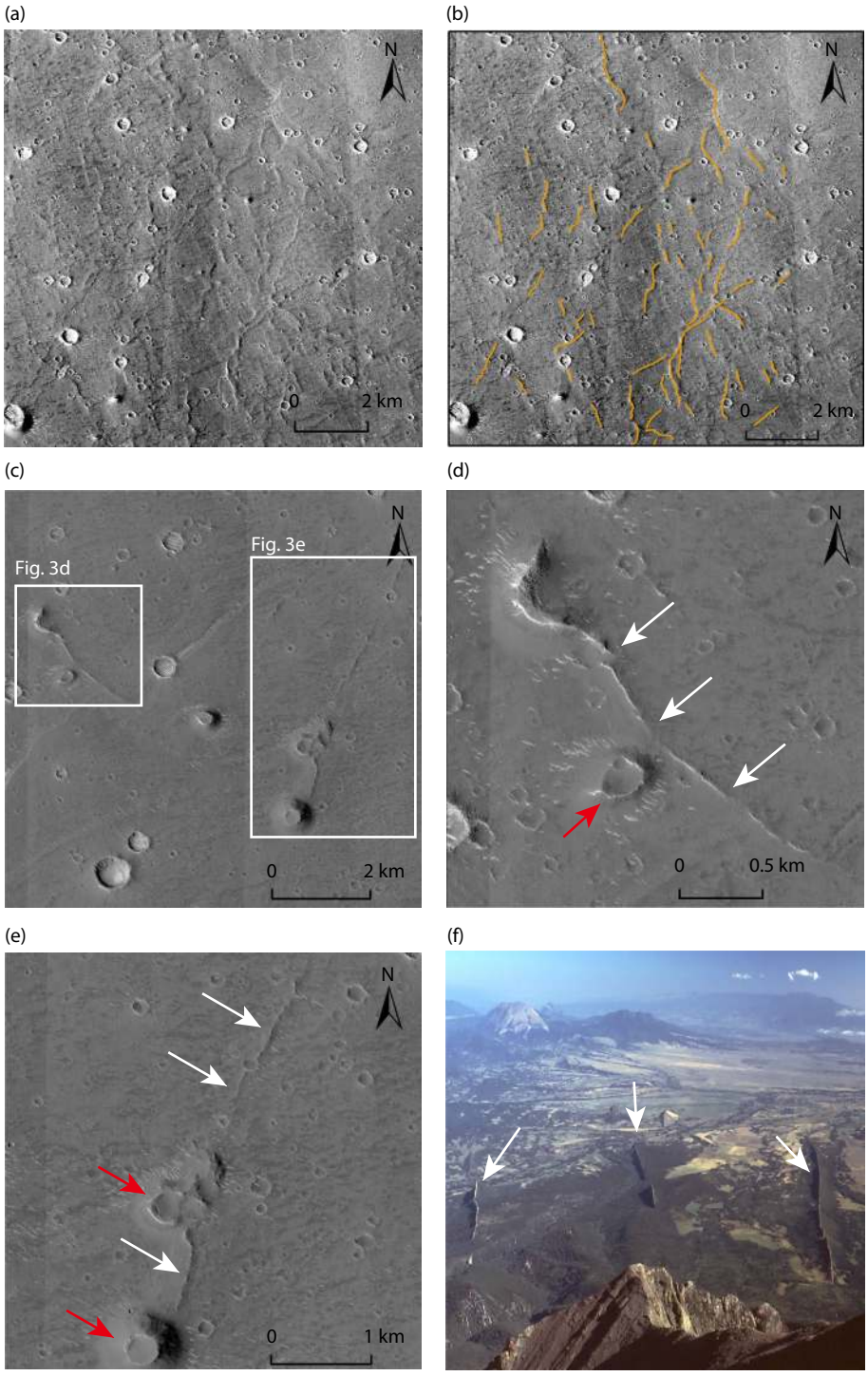

Figure 3. Examples of ridges shown by high-resolution imaging camera images. (a) A group of wrinkle ridges appears in this picture, and the orange lines in panel b outline them. (c) Example of ridges that are interpreted as dikes. The enlarged views of dikes outlined by the white boxes are shown in panels d and e, respectively. (d) A close-up view of the narrow, sharp-crested ridge, which is interpreted as an exhumed dike (white arrows), and a cone (red arrow) adjacent to this ridge. (e) Close-up view showing a dike (white arrows) crosscutting the cones (red arrows). (f) Photograph showing the narrow crests of exposed dikes (white arrows) on Earth from Colorado, USA. (Photograph by G. Thomas, available at commons.wikimedia.org/wiki/File: WestSpanishPeakCO.jpg.)

been interpreted as indicators of subsurface volatiles. For instance, an impact crater with rampart-like ejecta is indicative of the presence of abundant volatiles in the target materials (Mouginis-Mark, 1987). We found two rampart craters in our study area (Figure 1d). Figure 4a shows the southern rampart impact crater with a diameter of ~7.5 km and a depth of ~1.5 km. Figure 4b shows the northern rampart impact crater with a diameter of ~9 km and a depth of ~1.2 km. Their topographic profiles (Figures 4c and 4d) show clear symmetries of bowl-shaped interior walls, and the rampart craters have sharp, continuous rims. Both rampart craters show single-

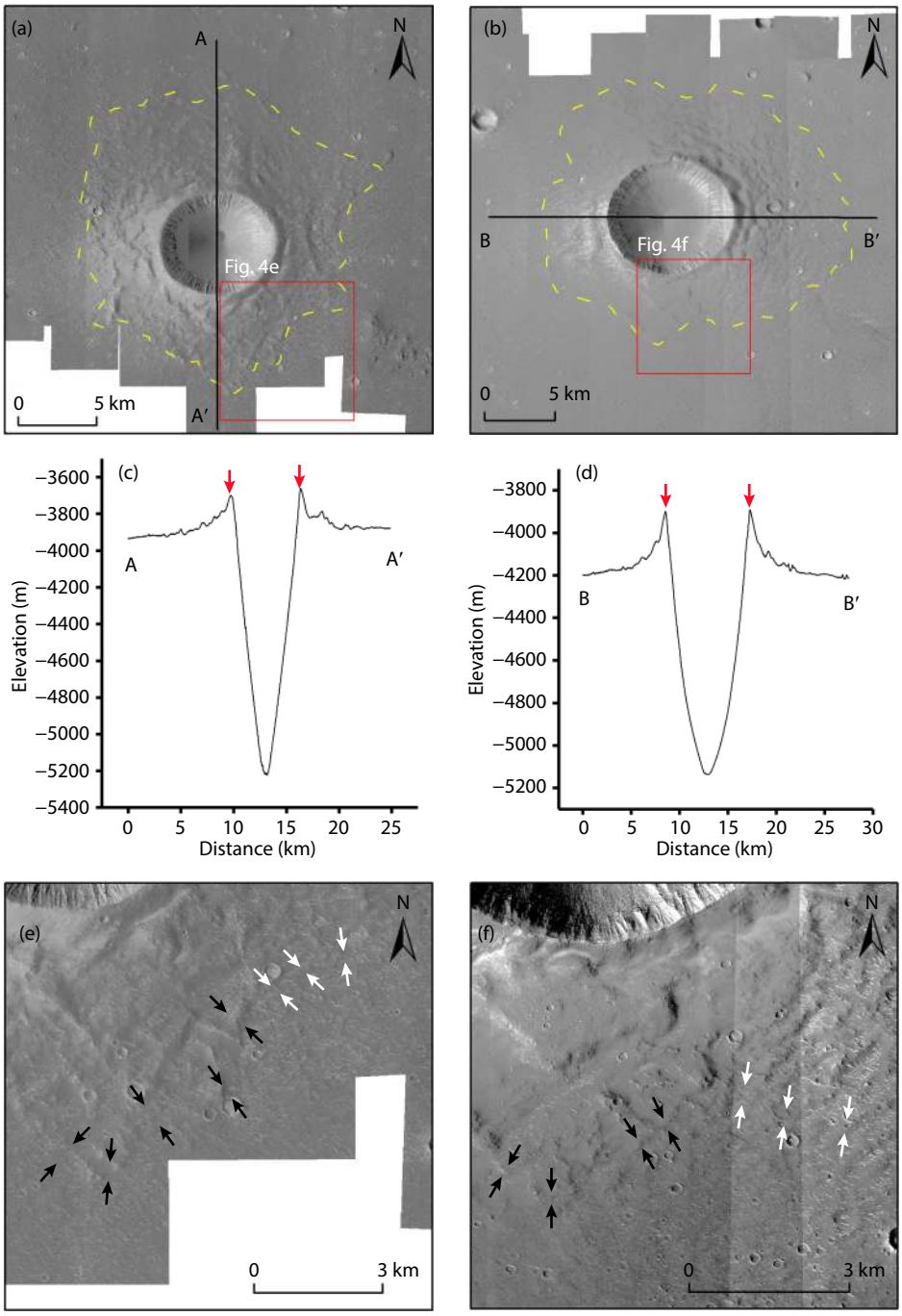

Figure 4. Two observed rampart craters in the landing area shown by high-resolution imaging camera (HiRIC) images: (a) the southern rampart crater, (b) the northern rampart crater. The yellow dashed lines outline the distal boundaries of the ejecta blankets. The red boxes indicate the locations of panels e and f, respectively. (c, d) HiRIC-derived topographic profiles, corresponding to A–A′ and B–B′ in panels a and b, respectively, which cross the centers of the two rampart craters. The red arrows indicate the crater rims. (e, f) Close-up views of the distal boundary of the ejecta blanket. The black arrows indicate the obvious edge, and the white arrows indicate the ambiguous edge.

layered ejecta (Damptz et al., 2010), and the edge of the ejecta is buried by dust materials or is eroded (denoted by the white arrows in Figures 4e and 4f). This observation suggests that the rampart craters are younger impact craters. Additionally, the AMA of the ejecta ranges between 1.15 and 1.19 Ga (Figure 5). The overall ejecta flow morphologies of rampart craters generally correlate with the presence of subsurface water ice (Mouginis-Mark, 1987; Barlow and Perez, 2003; Baloga et al., 2005). We also estimated the excavation depths of the potential subsurface volatiles, which range between ~0.24 and ~0.28 km ($d = 0.131D^{0.85}/3$, where d is the excavation depth and D is the current rim diameter of the crater; Barlow and Perez, 2003).

3.3 Mesas

Mesas are flat-topped, topographically high platforms with sloped sides (Chan et al., 2010; Ivanov et al., 2014). Figure 6 shows the

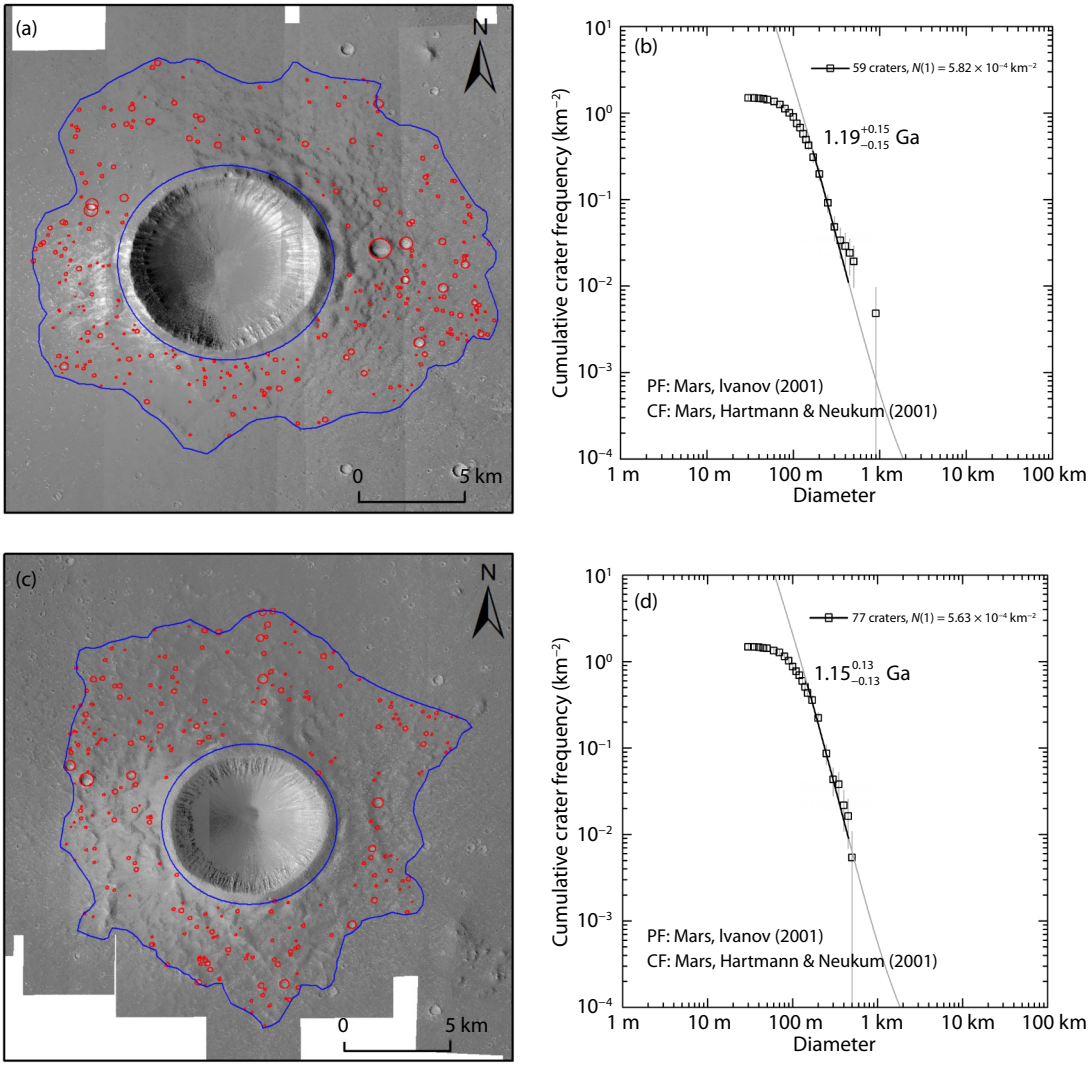

Figure 5. (a) The counted craters (red circles) on the northern rampart crater overlaying the high-resolution imaging camera (HiRIC) image. (b) The best fit of the corresponding crater size–frequency distribution (CSFD). (c) The counted craters (red circles) on the southern rampart crater overlaying the HiRIC image. (d) The best fit of the corresponding CSFD.

three observed flat-topped mesas, which vary in height from 120 to 180 m. The length of these mesas varies from 2,516 to 4,215 m, and the width of the mesas ranges from ~1,570 to 3,087 m. They do not resemble round mesas, which are common in the Martian outflow channels (Coleman, 2008). They are irregularly shaped platforms in the study area. Mesas in the fretted terrain are thought to have been formed from ice-facilitated mass wasting processes from ground or atmospheric sources (Carr, 2001). The study by Ivanov et al. (2014) suggests that isolated mesas with scalloped edges may indicate the friable materials of the upper plateaus and the possible presence of volatiles in etched flows. Mesas show scalloped edges separated from the surrounding contiguous layer (yellow dashed arrows in Figures 6a and 6c). The topographic contour maps of these mesas are closed (Figures 6b and 6d), and their elevations gradually decrease from the tops to the edges. The observation and topographic evidence indicate that the mesas are layered. Figure 6a shows a mesa with cones (black arrows in Figure 6a) and etched traces (white arrows in Figure 6a). They show a genetic spatial relationship. Some small impact craters are also located at the top of the mesas (black arrows in Figure 6c). We suspect that these layered mesas may be the erosion-resistant remnant materials, whereas the volatile-rich (or friable) materials could have been eroded and transported, as described by Carr (2001) and Ivanov et al. (2014).

3.4 Cones

The most significant observations in the study area are cones, which are common features in Utopia Planitia (De Pablo and Komatsu, 2009; McGowan, 2011). The most likely origins for these features are pingos, mud volcanoes, and igneous constructs, but their origins are still under discussion (Skinner and Tanaka, 2007; De Pablo and Komatsu, 2009; Lanz et al., 2010; Ivanov et al., 2014). Cones in our study area are widely distributed (Figure 1d) and have morphologically smooth surfaces covered with fine materials or dust. Most of the observed cones occupied the southern study area (Figure 2b). In total, 272 well-preserved circular cones have been identified in the landing area, with the basal diameters ranging from 178.9 to 1,206.6 m, the crater widths ranging from

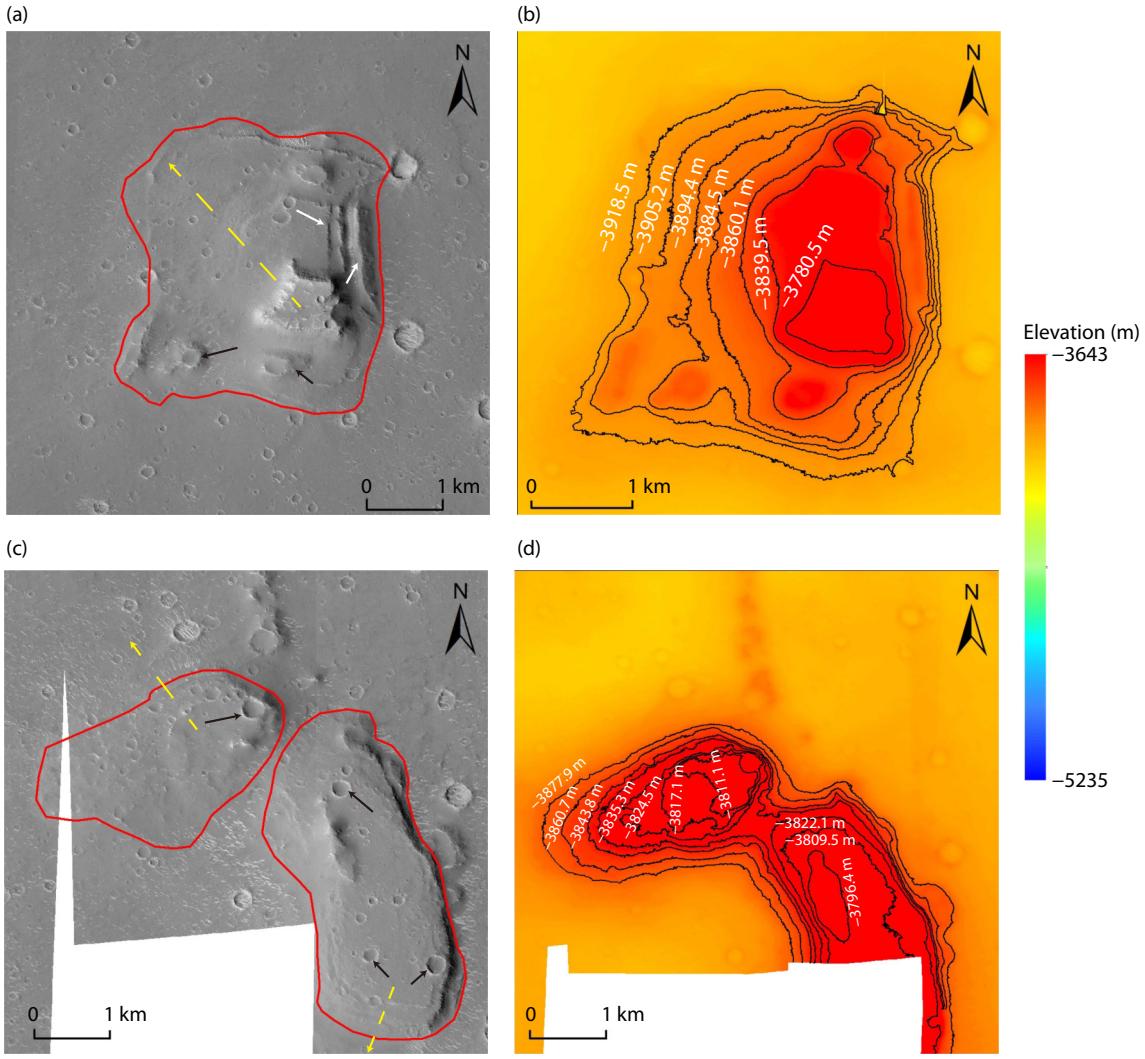

Figure 6. Typical mesas in the landing area. The red lines show the approximate boundaries of the mesas. The yellow dashed lines indicate the layered characteristic of the mesas. (a) A flat-topped, layered mesa with etched traces (white arrows) and cones (black arrows). (b) Topographic contour map of the mesa in panel a. The elevations are denoted in white. (c) Two adjacent mesas with small craters (black arrows) on the top. (d) Topographic contour map of the mesas in panel c. The elevations are denoted in white.

58.0–687.9 m, and the heights ranging from 10.5 to 90.8 m (Huang H et al., 2022). In the study area, the cones are isolated (Figure 7a), are clustered (Figure 7b), or form chains with a ridge (Figure 7c). In our previous study, we conducted a quantitative analysis of the cones in the landing area and speculated that they are most likely mud volcanoes (Huang H et al., 2022). Mud volcanoes are generally built with a mixture of gas, liquid water, and sediments (Hemmi and Miyamoto, 2017; Brož et al., 2019) that originated from depth (Kopf, 2002). If the landing area cones were truly associated with mud volcanoes, subsurface sediment mobilization could have occurred in the landing area in the early time, which may provide vital clues to the northern ancient ocean hypothesis.

3.5 Troughs

Troughs are common in the northern portion of the study area and are not evenly distributed (Figures 1d and 2c). Troughs in our study area are 1.2–10.0 km in length, up to 20 m in depth, and 90–840 m in width, and they are oriented in different orientations, such as north–south, east–west, and northwest–southeast. Several morphologic types characterize the prominent troughs: (1) Figure 8a shows a narrow linear trough with a smooth surface in a cratered terrain; (2) Figure 8b shows a sinuous angular trough with prominent branching troughs; (3) Figure 8c shows a trough (like etched flow traces) underneath the cones, indicating that this trough is the same age as the surrounding cones or older; and (4) Figure 8d shows a linear trough filled by transverse aeolian ridges (TARs) with an irregularly shaped crater superposed and suggests that the surface features (not only troughs) may have been modified. However, none of the troughs in the landing area created polygons, although polygonal troughs or polygonal terrains are one of the distinctive features in Utopia Planitia (Hiesinger and Head, 2000; Cooke et al., 2011). Thus, the troughs in our study area may not be the polygonal troughs commonly found in Utopia Planitia.

3.6 Additional Observations

The topographic configuration of the study area shows the differ-

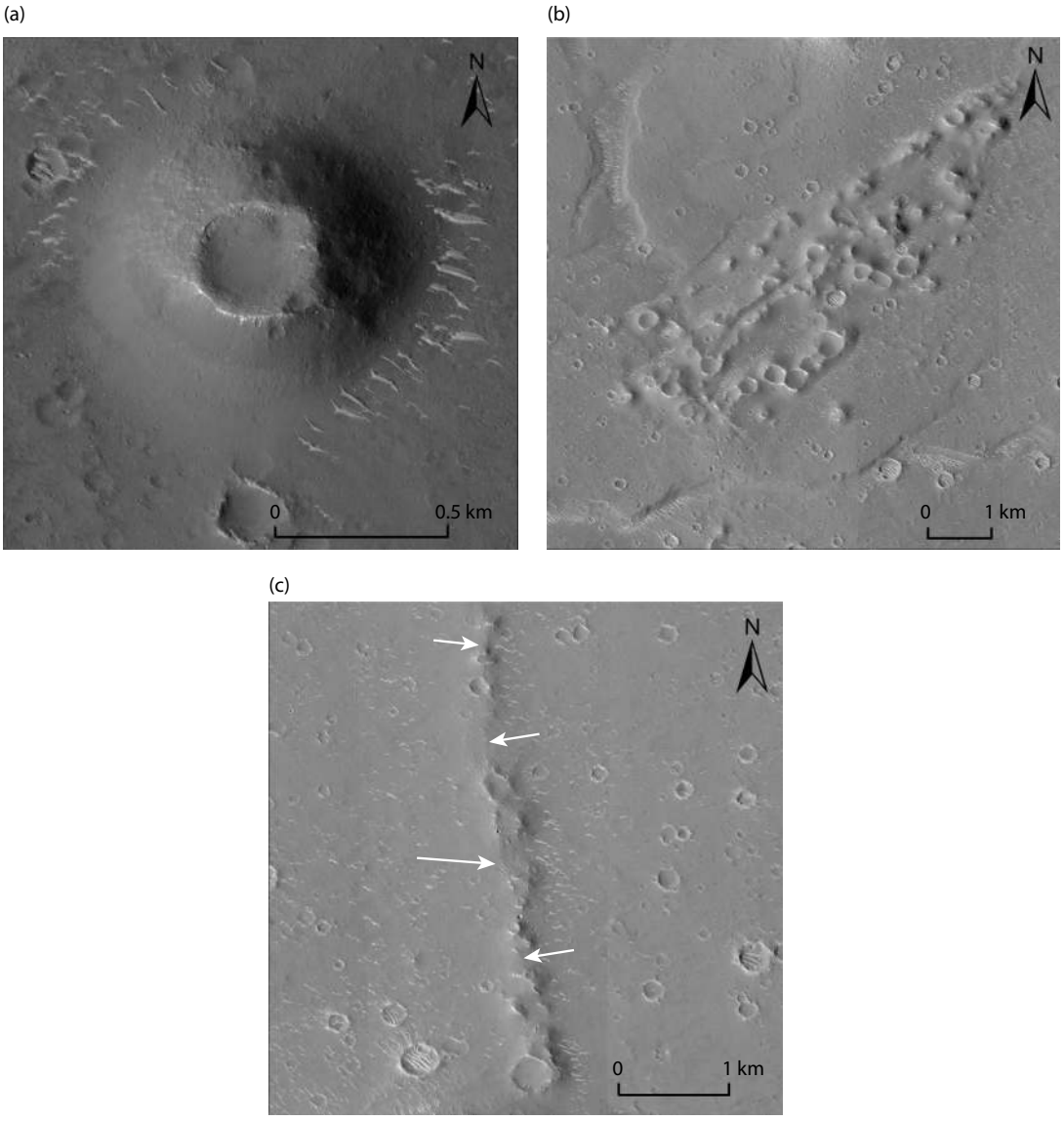

Figure 7. Examples of the cones in the landing area shown by high-resolution imaging camera images. (a) An isolated cone with a crater diameter of ~340 m, a basal diameter of ~980 m, and a height of ~82 m. (b) A cone cluster. (c) A cone chain with a ridge (white arrows).

ence between the southern and northern areas, and the southern portions are topographically higher than the northern portions (Figure 1b). In the southern study area, a small depression (~60 m deep) with a noticeably gentler slope scarp (~39.266 km long, 1.9°–8° in flank slope) (Figures 9a and 9b) appears in Figures 1b and 1c. Many cones are adjacent to the scarp, and they may show a genetic spatial relationship (Figure 10). We measured 11 elevation profiles of the transects (Figure 9a) and found that the slope of the scarp is steep in the middle but gentle at both ends. Figure 9c shows the transect elevation profiles, which correspond to the steep and gentle portions of the scarp, with differences occurring in the flank slopes. In the steepest portion of the scarp, the upper portion is steeper than the lower portion. Potential degradation (possible mass wasting processes) may have occurred at the scarp. According to our observations and analyses, this small depression tends to deepen from the edge (i.e., the scarp). Both ground uplift and subsidence can lead to a topographic depression. Figure 11 shows the topographic analysis of the depression. As mentioned, the southern landing area is topographically higher than the northern landing area, and the −4,100 m contour line (green line in Figure 11) can roughly divide the landing area into two parts. The depression (red dashed box in Figure 11) with the same elevation edge (blue line in Figure 11) appears in the southern landing area. In the case of ground uplift, it should be an overall uplift of a relatively continuous layer (e.g., the whole of the southern landing area) rather than a depression in a portion of the southern landing area. On the contrary, ground subsidence (e.g., caused by potential local magma chamber evacuation or geothermal heat-eroded subsurface volatiles) is more likely to cause a topographic depression in a single layer. Moreover, there is not enough evidence to exclude the depression as having been formed from the accumulation of natural materials (e.g., lava flows, mudflows) such that the surrounding areas are higher than the depression. For example, Mills et al. (2021) interpreted the observed lobate margins in the TW-1 Zhurong landing region as past lava or mud flow boundaries.

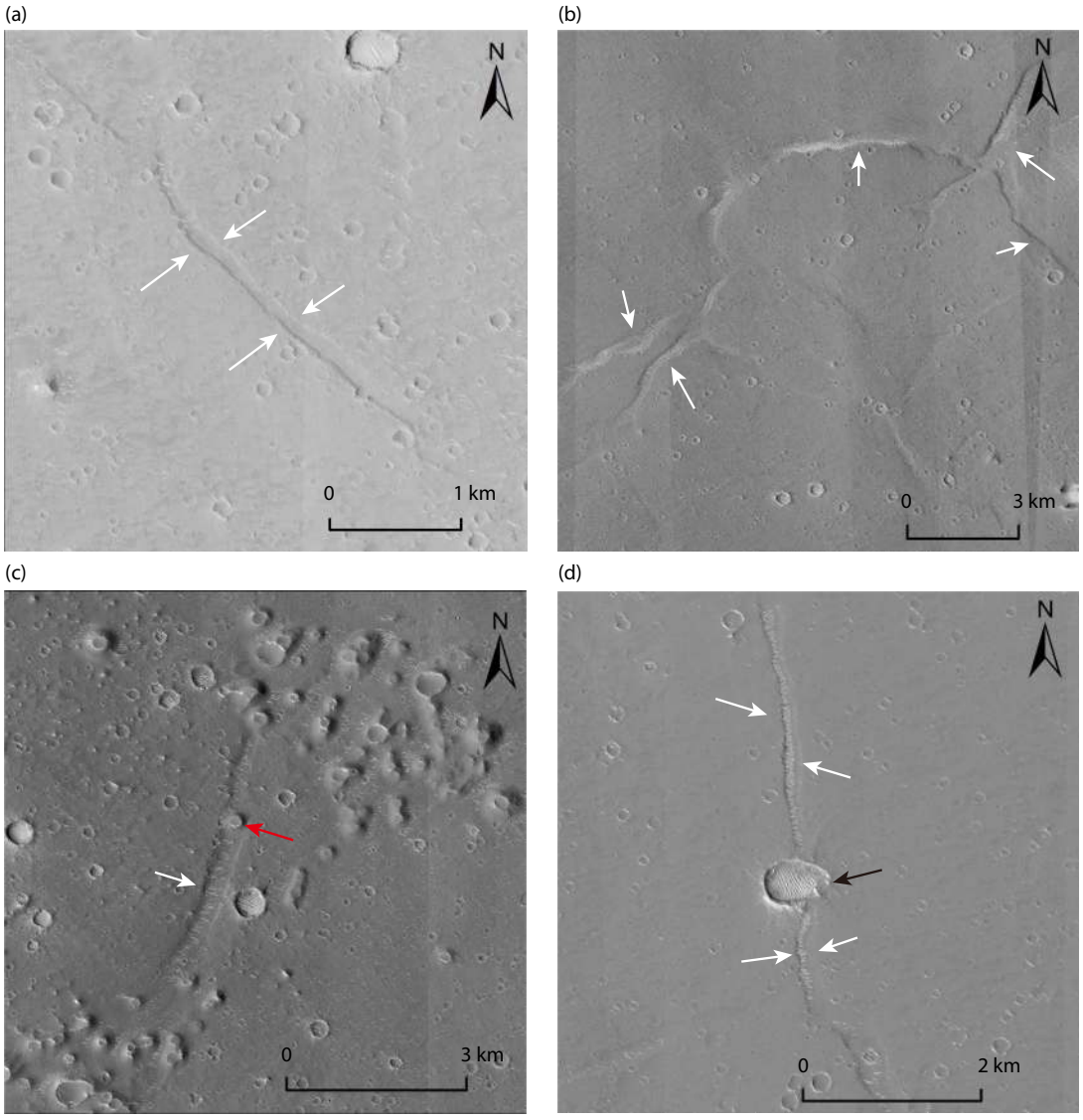

Figure 8. Troughs in the landing area shown by high-resolution imaging camera images. All the troughs are denoted by white arrows. (a) A narrow and shallow linear trough with a range from 110 to 150 m wide and ~7 m deep. (b) Sinuous angular trough with branching troughs. (c) A trough up to ~400 m wide and ~20 m deep that appears in a cone field. A cone sits (red arrow) inside the trough. (d) A trough ~100 m wide and ~10 m deep that was filled by transverse aeolian ridges. An irregular crater (black arrow) was superposed on the trough.

Here, we test the formation mechanism of the depression caused by the removal of subsurface volatile materials. Wu X et al. (2021) suggested that the excavation depth of subsurface volatiles in Utopia Planitia could range from 167 to 714 m. We assume that the ice storage thickness is 714 m – 167 m = 547 m. Based on the crust porosity models (Clifford, 1993; Hanna and Phillips, 2003, 2005), the crustal porosity at depths shallower than ~1 km is 15% to 20% (Figure 12). Under ideal conditions, all the pore space would have been completely filled with ice and completely compacted after the ice disappeared, then the upper 1 km with 15% to 20% porosity would yield 82–109 m of collapse. Thus, it is reasonable that the disappearance of subsurface ice caused the ground subsidence and yielded small depressions in the landing area (~60 m depth).

Transverse aeolian ridges, a term originated by Bourke et al. (2003), describes the linear to curvilinear bedforms on Mars, forming either large ripples or small dunes. They are usually ~10-m-scale, ripple-like aeolian bedforms on Mars (Berman et al., 2011). Transverse aeolian ridges up to ~1 m high are widely distributed in the study area. Figures 13a and 13b show the east–west-trending TARs surrounding the landing site, suggesting an north–south-trending regional wind direction in the past. This indicates that the surface of the landing area has undergone extensive aeolian processes. Figure 13c shows a barchan-like TAR near the Zhurong rover.

4. Surface Material Characteristics and Absolute Model Ages

Our morphologic observations and analyses support the possibility of past igneous- and water ice-related activities. We attempted to find more evidence for volcanic materials and water ice-related (e.g., hydrous minerals) materials in the study area by orbital remote-

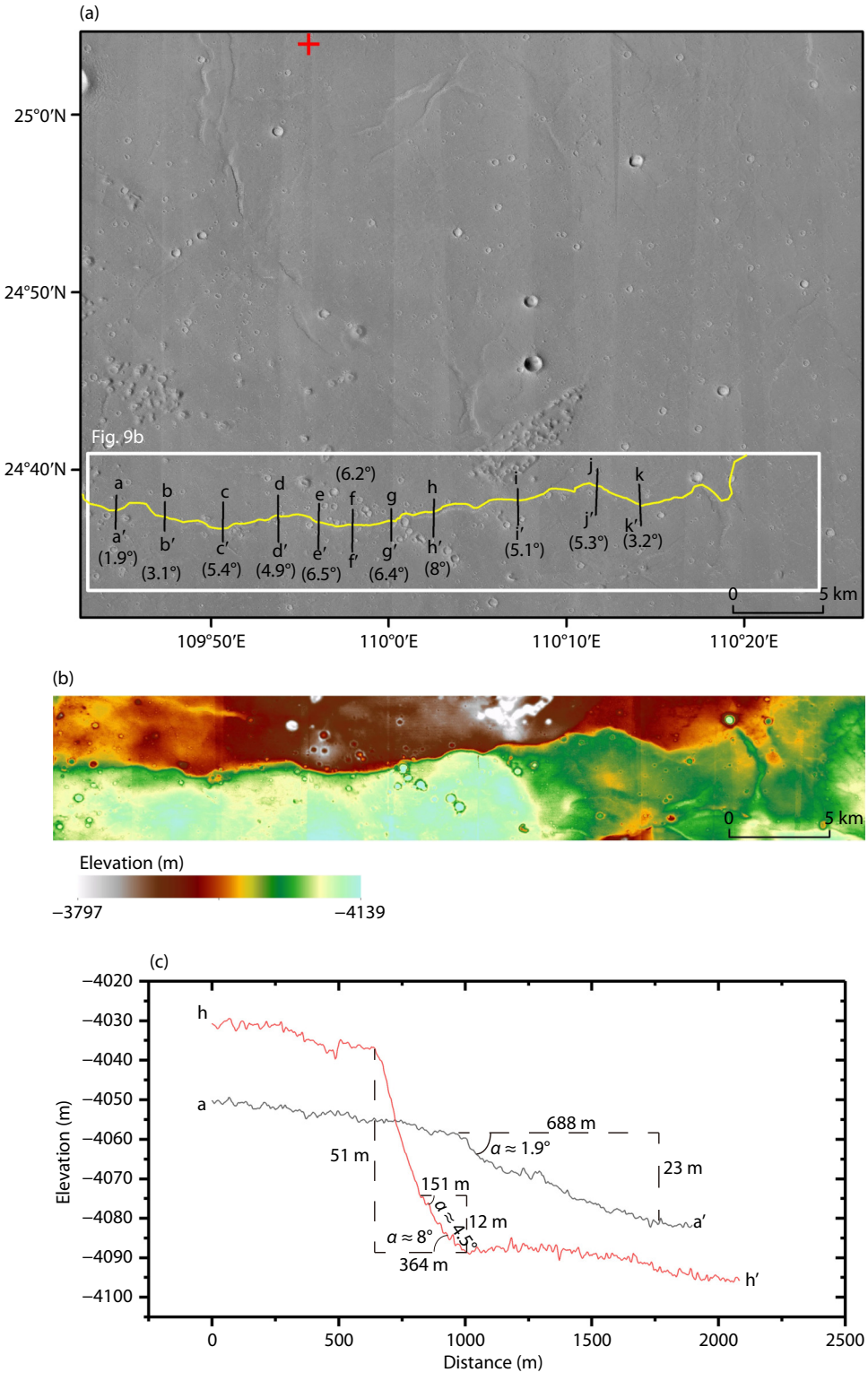

Figure 9. (a) High-resolution imaging camera (HiRIC) images show the scarp ~27 km away from the landing site, which belongs to the small depression. Some cones are adjacent to the scarp. The yellow line denotes the scarp. The black lines indicate topographic profiles across the scarp, and the flank slopes of the scarp are adjacent to them. The white box indicates the location of panel b. The red cross indicates the landing site. (b) HiRIC topography data show the topographical characteristics surrounding the scarp. (c) The selected two transect profiles of a–a′ and h–h′ represent the steepest and gentlest portions of the scarp, respectively. The topographic profile of h–h′ indicates that the lower half of the scarp has a gentler slope (or perhaps a more degraded one). Note *α* indicates the flank slope.

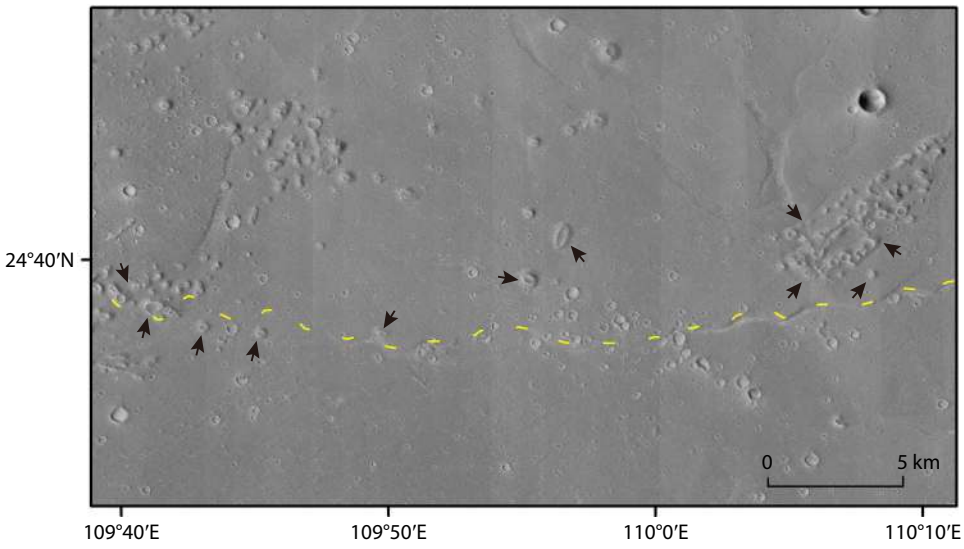

Figure 10. High-resolution imaging camera image showing that the cones are adjacent to the scarp. The black arrows indicate the cones, and the yellow dashed line outlines the scarp.

sensing approaches; however, it is difficult to obtain unambiguous information because of the lack of high-quality spectral images (e.g., compact reconnaissance imaging spectrometers for Mars [CRISM] targeted data) in this region. The global dust cover index (DCI) map shows a dust-covered surface of Utopia Planitia (Ruff and Christensen, 2002), and the pervasive dust cover heavily obscures the spectral features. Figure 14 shows the DCI values of the landing area based on thermal emission spectrometer data (Ruff and Christensen, 2002). The threshold at ~0.94 is for dust-covered surfaces and that at ~0.96 is for dust-free surfaces, whereas intermediate DCI values represent partially dust-covered surfaces. Thus, there are few dust-free surfaces in the study area, and most landing areas are dust-covered surfaces to differing degrees. A panorama (Figure 13c) of the surface environment surrounding the Zhurong rover also indicates a dust-covered surface, supporting the above-mentioned observation.

The landing area lies in the Late Hesperian lowland unit (Tanaka et al., 2014; Liu JJ et al., 2022). Martian northern lowlands show a complex resurfacing history, especially resurfaced by the VBF (Tanaka et al., 2003). We derived the AMAs of the landing area surface based on the CSFD, and the counted craters are shown in Figure 15a. The AMAs of the landing area have a Late Hesperian age of ~3.3 Ga (Figure 15b), whereas the estimated younger age (~1.6 Ga) possibly reflects the later resurfacing events. The derived AMAs in this work are consistent with previous results (Ivanov et al., 2014; Wu X et al., 2021). No ghost craters, which would indicate a more ancient stratum, were observed in the landing area. However, the AMA of the terrain predating the emplacement of the VBF is ~3.7 Ga as estimated by the ghost craters (Ivanov et al., 2014; Wu X et al., 2021). Thus, we accept the AMA of ~3.7 Ga of a more ancient stratum in our study area. Our CSFD analysis of the landing area shows complex stratigraphic relationships.

5. Orbiter-Based Interpretations and Discussion

As mentioned, the geologic background of Utopia Planitia indicates a complex regional geologic evolutionary history. The two main factors of thermal effects and water ice interactions could be responsible for creating the surface geologic features of Utopia Planitia. Head et al. (2002) proposed that the bulk of the northern plains are Early Hesperian volcanic ridged plains. The possibility that water ice-related activities (e.g., a putative northern ocean, the VBF) existed in Utopia Planitia is also worthy of consideration. According to the results of our observations and analyses of the landing area, we also suspect, based on remote-sensing approaches, that thermal influences and water ice may have played an important role in building the surface geomorphologic features of our study area. Therefore, to provide the most plausible interpretation for the surface of the landing area, we provide four possible formational scenarios and test them:

(1) *Scenario A — Thermal and water ice-related influences.* In this formation scenario, underground thermal influences and water ice are the two key factors. We observed igneous-related features, such as dikes and wrinkle ridges. Rampart craters and mesas indicate the presence of subsurface volatiles or friable materials. Thus, water ice may be the important factor in forming some observed surface geomorphologic features. This scenario can also explain the proposed mud volcanoes in the landing area well. Troughs in our study area are not easily explained by a certain formation mechanism; however, we can exclude them as polygonal troughs. Likewise, wind processes cannot explain sinuous branching troughs (Figure 8b). In this scenario, fluid-related activities (e.g., lava tubes, magma–water ice interactions) are plausible formation mechanisms to explain troughs in our study area. The small depression with a scarp in the middle of the landing area may be related to geothermal heating and water ice in this scenario (e.g., magma chamber evacuation, geothermal heat-eroded friable materials, sublimation of ice). Therefore, scenario A can explain almost all the surface geomorphologic features in the landing area.

(2) *Scenario B — Thermal without water ice-related influences.* In this scenario, we suggest that water ice does not affect the surface of the landing area. The observed dikes and wrinkle ridges can be

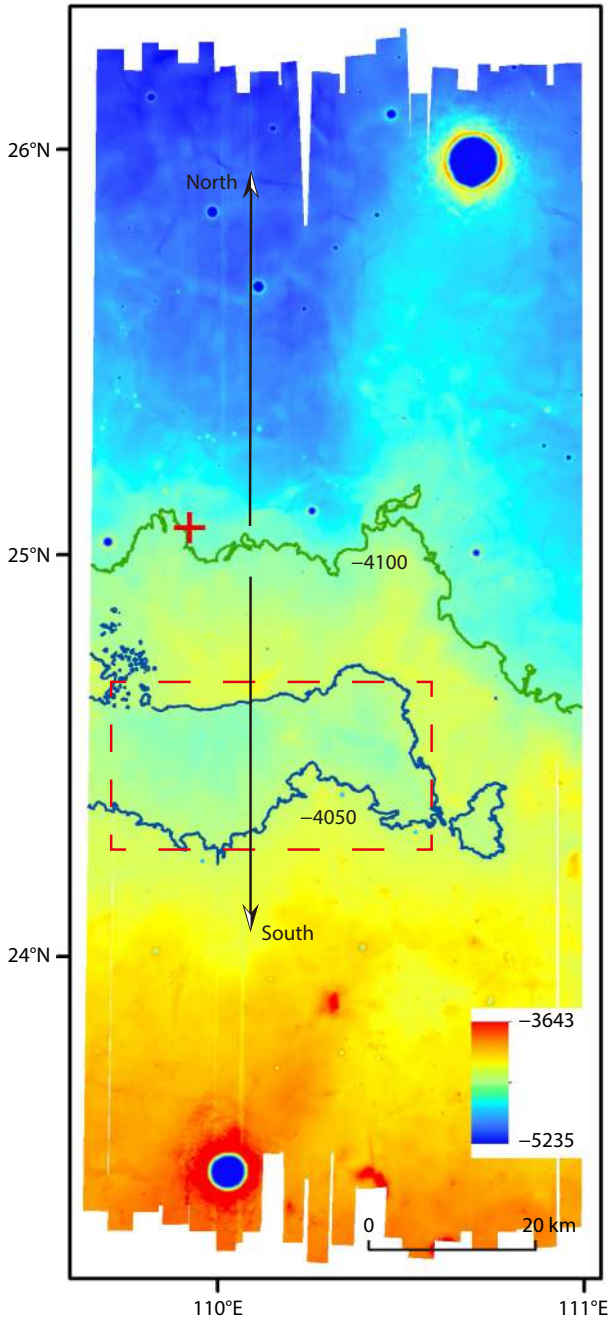

Figure 11. Topographic analysis of the depression. The red cross indicates the landing site. The green line denotes the –4,100 m contour line, and the blue line denotes the –4,050 m contour line (the edge of the depression). The red dashed box indicates the depression. The arrows denote the southern and northern landing areas, respectively.

explained well in this scenario as the products of igneous activity. However, the presence of rampart craters and mesas, which need volatiles, is inconsistent with igneous activity. This scenario is also inconsistent with the geologic setting of Utopia Planitia, where water ice may exist, although the southern edge of Utopia Planitia may contain lower abundances of these volatiles. Thus, this scenario is not the feasible formational scenario.

(3) *Scenario C — Water ice-related without thermal influences*. In this scenario, we suggest that thermal influences do not affect the surface of the landing area. We can explain cones as mud volcanoes. Skinner and Mazzini (2009) provided five possible formational scenarios for Martian mud volcanism, some of which require heat sources and some of which do not. Troughs can be explained as a consequence of fluid activities or the sublimation of ice. The sublimation of ice can also explain the existence of small depressions. However, apparently igneous-related features, such as dikes and wrinkle ridges, are inconsistent with this scenario. Therefore, scenario C, like scenario B, cannot explain all the surface geomorphologic features.

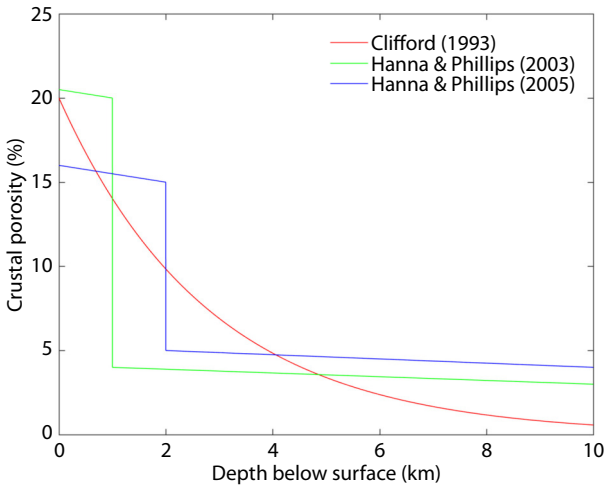

Figure 12. Various models of crustal porosity with depth below the Martian surface.

(4) *Scenario D — Others*. In this scenario, we do not invoke either thermal or water ice-related influences. Thus, the landing area may undergo various candidate geologic processes, such as impact-related processes, wind processes, and tectonic processes. Here, we conduct analyses of the most likely formation mechanism of every observed landform in the landing area. First, the impact-related processes can explain the ring-shaped relief, but not the cones (De Pablo and Komatsu, 2009). Second, wind processes can produce ridge-like features. If the ridges are aeolian productions, they may display unusual spatial distribution, similar to yardangs (Zimbelman and Griffin, 2010). However, the morphology of the ridges in our study area varies, and the spatial distribution of ridges is sparse. In addition, wind processes do not adequately explain other geomorphologic features here. Finally, the tectonic processes may generate troughs. The gentler scarp slope and the size of troughs are possibly inconsistent with the formational scenario of typical tectonic processes. Thus, we suspect that scenario D could not explain most of the features without thermal influences or water ice.

According to our analyses, scenario A explains most of the surface geomorphologic features. Therefore, we suggest that the formation of surface geomorphologic features is related to igneous-related processes that can provide thermal energy and potentially water ice, which may also have been present in building the original edifices of the landing area surface. In addition, we do not observe either shield volcanoes (Carr, 1973) or eruptive fissures (Glaze et al., 2011), which could produce explosive volcanism.

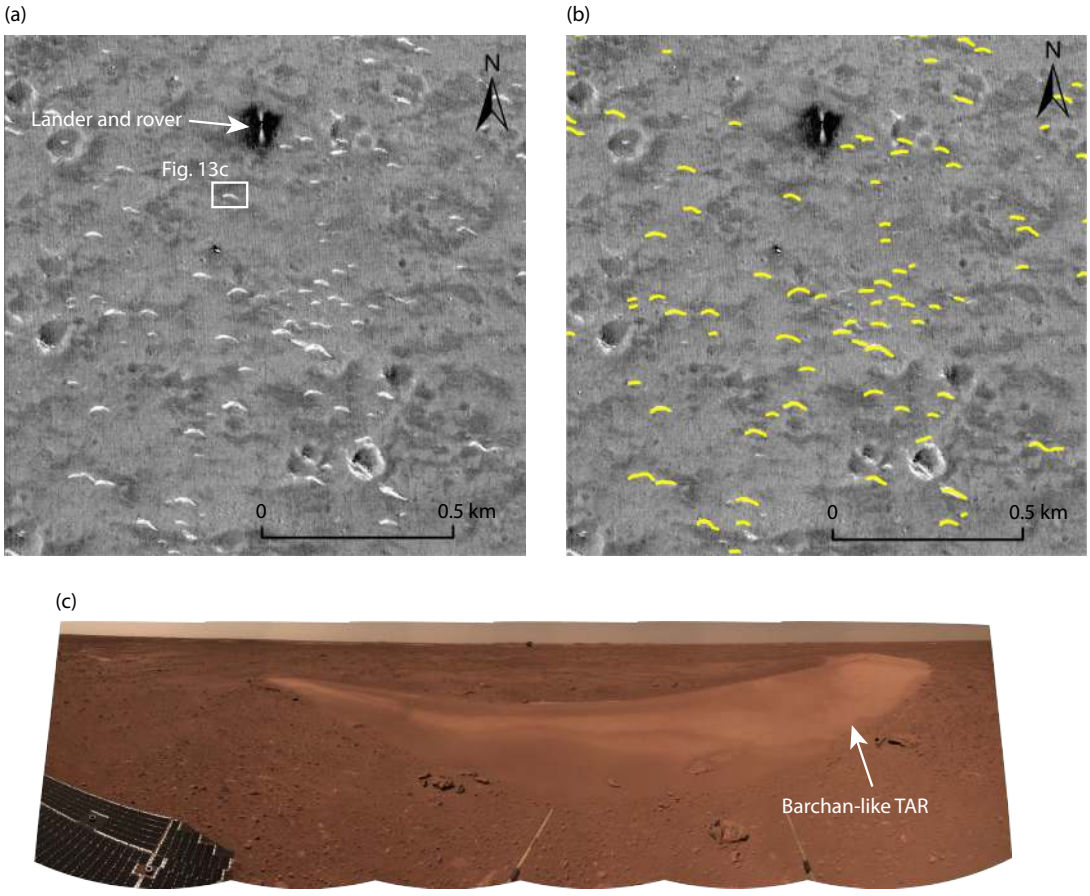

Figure 13. (a) High-resolution imaging camera image shows the east–west-trending transverse aeolian ridges (TARs) surrounding the landing site. (b) The yellow lines outline them. The white box indicates the approximate location of panel c. (c) The panorama shows a barchan-like TAR ahead of the Zhurong rover.

Unambiguous traces of volcanic activity in Utopia Planitia are missing (Lanz et al., 2010), and our study area has very few unambiguous volcanic or igneous traces. Later resurfacing events and aeolian processes could have buried and modified the primordial volcanic or igneous edifices.

The study area of this research lies outside any of the large volcanic provinces (Werner, 2009). Ivanov et al. (2014) did not observe dikes or dike swarms in their study area (including our study area), which usually indicates subsurface heat sources. We observed ridges in our study area that were interpreted as dike intrusions. However, there is insufficient evidence to support the presence of a magma chamber beneath the landing area, which could provide a stable heat source. Our CSFD analysis shows that the surface of the VBF in the landing area has a Late Hesperian age of ~3.3 Ga, and the AMA of terrain predating the emplacement of the VBF is ~3.7 Ga (Early Hesperian; Ivanov et al., 2014). Although we cannot determine the relationship between the stratigraphic age of the landing area and the age of the surface geomorphologic features, in scenario A, the best time to build major edifices in the landing area was during the Hesperian period, when Martian volcanism continued at a relatively high average rate (Carr and Head, 2010).

The observed igneous-related features (e.g., dikes, wrinkle ridges) and water ice-related features (e.g., rampart craters, mesas) indicate that the landing area is a geologically complex region. The Zhurong rover has carried six scientific payloads (Li CL et al., 2021), such as the multispectral camera (MSCam), Mars surface composition detector (MarSCoDe), and Mars rover penetrating radar (RoPeR). Now the Zhurong rover is heading toward the south, and the surface in situ features (e.g., TARs, cones, troughs, dust) of the landing area will be studied and discussed in depth in future works with scientific data from the rover. The additional information (e.g., subsurface structures, surficial material properties, geochemical and geophysical properties) from the in situ investigation will help us better understand the local geologic history. For example, Liu Y et al. (2022) recently found hydrated sulfate and silica materials in the landing area by using the short-wave infrared spectral data obtained by the Zhurong rover. Furthermore, possible investigations for high-resolution gravity fields of the landing area by using the gravity anomaly data may also provide new insights into the proposed formational scenario (Genova et al., 2016).

6. Conclusions

Herein, to gain a more complete and detailed understanding of the TW-1 landing area, we surveyed the surface of the TW-1 landing area based on orbital imagery data. We present a detailed geomorphologic map of the landing area. Five major morphologic features were observed: rampart craters, mesas, ridges, troughs,

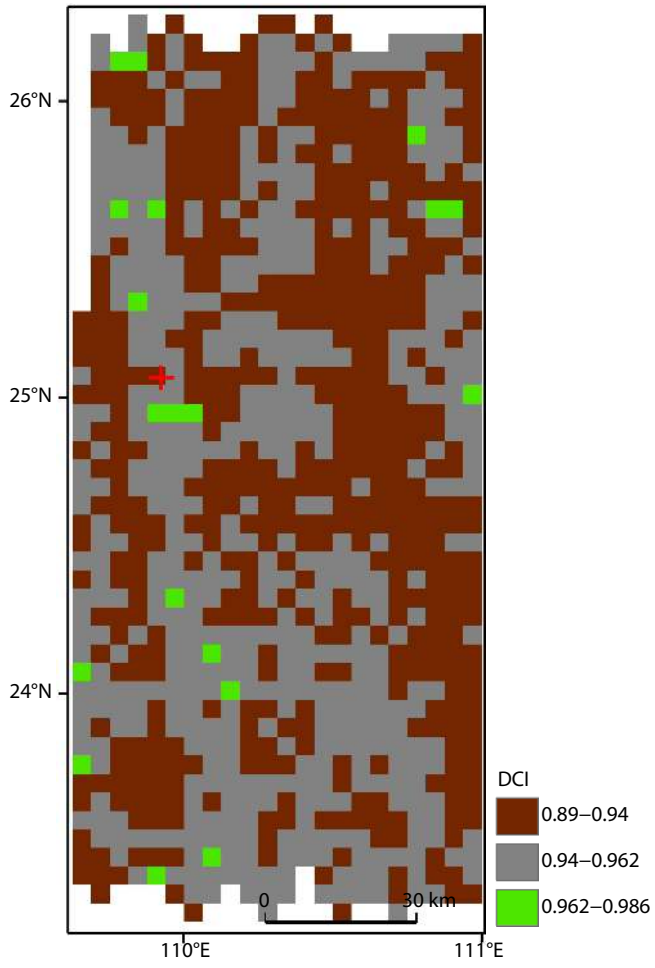

Figure 14. Dust cover index (DCI) map of the landing area. The red cross indicates the landing site.

and cones. The observed igneous-related features (e.g., dikes, wrinkle ridges) may provide valuable insights into the geothermal heat source (e.g., magma chamber) in Utopia Planitia. The water ice-related features indicate that volatiles may have existed in this area in a historic period. We present a feasible formational scenario for the observed surface geomorphologic features: thermal influences and water ice interactions played important roles in forming the primordial surface landforms, and possibly igneous processes may have operated in the landing area. These features were subsequently buried and modified by later resurfacing events and wind processes. Future in situ exploration will provide additional evidence to test our proposed scenario because some issues are still under discussion, such as whether a stable subsurface heat source (magma chamber) ever existed beneath Utopia Planitia.

Acknowledgments

All HiRIC data used in this work are available at https://moon.bao.ac.cn/web/enmanager/zygj. Data sets generated or analyzed during this study are available from the corresponding author upon reasonable request. This study was supported by the Key Research Program of the Chinese Academy of Sciences (Grant No. ZDBS-SSW-TLC001) and the National Natural Science Foundation (Grant No. 11803056).

References

Baloga, S. M., Fagents, S. A., and Mouginis-Mark, P. J. (2005). Emplacement of Martian rampart crater deposits. *J. Geophys. Res.*: *Planets*, *110*(E10), E10001. https://doi.org/10.1029/2004JE002338

Barlow, N. G., and Perez, C. B. (2003). Martian impact crater ejecta morphologies as indicators of the distribution of subsurface volatiles. *J. Geophys. Res.*: *Planets*, *108*(E8), 5085. https://doi.org/10.1029/2002JE002036

Berman, D. C., Balme, M. R., Rafkin, S. C. R., and Zimbelman, J. R. (2011). Transverse Aeolian ridges (TARs) on Mars II: distributions, orientations, and ages. *Icarus*, *213*(1), 116–130. https://doi.org/10.1016/j.icarus.2011.02.014

Bilotti, F., and Suppe, J. (1999). The global distribution of wrinkle ridges on Venus. *Icarus*, *139*(1), 137–157. https://doi.org/10.1006/ICAR.1999.6092

Bourke, M. C., Wilson, S. A., and Zimbelman, J. R. (2003). The variability of transverse aeolian ridges in troughs on Mars. In *LPSC XXXIV*.

Brož, P., Hauber, E., Van De Burgt, I., Špillar, V., and Michael, G. (2019). Subsurface sediment mobilization in the southern Chryse Planitia on Mars. *J. Geophys. Res.*: *Planets*, *124*(3), 703–720. https://doi.org/10.1029/2018JE005868

Buczkowski, D. L., Seelos, K. D., and Cooke, M. L. (2012). Giant polygons and circular graben in western Utopia basin, Mars: exploring possible formation mechanisms. *J. Geophys. Res.*: *Planets*, *117*(E8), E08010. https://doi.org/10.1029/2011JE003934

Carr, M. H. (1973). Volcanism on Mars. *J. Geophys. Res.*, *78*(20), 4049–4062. https://doi.org/10.1029/JB078I020P04049

Carr, M. H. (2001). Mars Global Surveyor observations of Martian fretted terrain. *Journal of Geophysical Research*: *Planets*, *106*(E10), 23571–23593. https://doi.org/10.1029/2000JE001316

Carr, M. H., and Head, J. W., III. (2010). Geologic history of Mars. *Earth Planet. Sci. Lett.*, *294*(3–4), 185–203. https://doi.org/10.1016/J.EPSL.2009.06.042

Chan, M. A., Ormö, J., Murchie, S., Okubo, C. H., Komatsu, G., Wray, J. J., McGuire, P., McGovern, J. A., and The HiRISE Team. (2010). Geomorphic knobs of Candor Chasma, Mars: new Mars reconnaissance orbiter data and comparisons to terrestrial analogs. *Icarus*, *205*(1), 138–153. https://doi.org/10.1016/j.icarus.2009.04.006

Chicarro, A. F., Schultz, P. H., and Masson, P. (1985). Global and regional ridge patterns on Mars. *Icarus*, *63*(1), 153–174. https://doi.org/10.1016/0019-1035(85)90025-9

Clifford, S. M. (1993). A model for the hydrologic and climatic behavior of water on Mars. *J. Geophys. Res.*: *Planets*, *98*(E6), 10973–11016. https://doi.org/10.1029/93JE00225

Coleman, N. (2008). Round mesas on the floor of Ravi Vallis, Mars—are they igneous intrusions?. In *39th Lunar and Planetary Science Conference*. League City: LPSC XXXIX.

Cooke, M., Islam, F., and McGill, G. (2011). Basement controls on the scale of giant polygons in Utopia Planitia, Mars. *J. Geophys. Res.*: *Planets*, *116*(E9), E09003. https://doi.org/10.1029/2011JE003812

Costard, F., Sejourne, A., Kargel, J., and Godin, E. (2016). Modeling and observational occurrences of near-surface drainage in Utopia Planitia, Mars. *Geomorphology*, *275*, 80–89. https://doi.org/10.1016/J.GEOMORPH.2016.09.034

Damptz, A. L., Glaze, L. S., and Baloga, S. M. (2010). A new analysis of rampart crater ejecta thickness profiles on Mars. In *41st Lunar and Planetary Science Conference*.

De Pablo, M. Á., and Komatsu, G. (2009). Possible pingo fields in the Utopia basin, Mars: geological and climatical implications. *Icarus*, *199*(1), 49–74. https://doi.org/10.1016/J.ICARUS.2008.09.007

Genova, A., Goossens, S., Lemoine, F. G., Mazarico, E., Neumann, G. A., Smith, D. E., and Zuber, M. T. (2016). Seasonal and static gravity field of Mars from MGS, Mars Odyssey and MRO radio science. *Icarus*, *272*, 228–245. https://doi.org/10.1016/j.icarus.2016.02.050

Glaze, L. S., Baloga, S. M., and Wimert, J. (2011). Explosive volcanic eruptions from linear vents on Earth, Venus, and Mars: comparisons with circular vent eruptions. *J. Geophys. Res.*: *Planets*, *116*(E1), E01011. https://doi.org/10.1029/

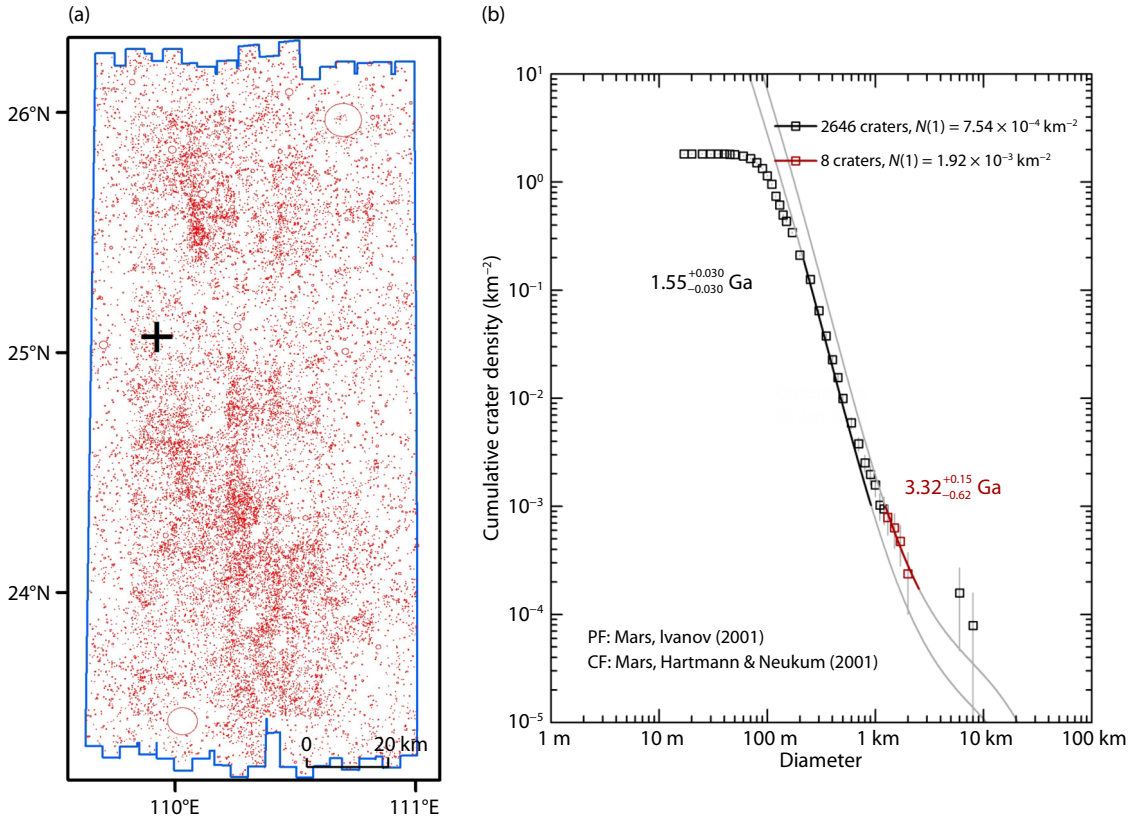

Figure 15. (a) This map shows the count area (blue outline) for crater size–frequency distribution measurements. The counted craters are outlined with red circles. The black cross indicates the landing site. (b) Model ages derived from crater statistics for the landing area surface.

2010JE003577

Greeley, R., and Thompson, S. D. (2003). Mars: Aeolian features and wind predictions at the Terra Meridiani and Isidis Planitia potential Mars Exploration Rover landing sites. *Journal of Geophysical Research: Planets*, 108(E12). https://doi.org/10.1029/2003JE002110

Hanna, J. C., and Phillips, R. J. (2003). A new model of the hydrologic properties of the Martian crust and implications for the formation of valley networks and outflow channels. In *34th Annual Lunar and Planetary Science Conference*. League City.

Hanna, J. C., and Phillips, R. J. (2005). Hydrological modeling of the Martian crust with application to the pressurization of aquifers. *J. Geophys. Res.: Planets*, *110*(E1), E01004. https://doi.org/10.1029/2004JE002330

Hartmann, W. K., and Neukum, G. (2001). Cratering chronology and the evolution of Mars. *Space Sci. Rev.*, *96*(1–4), 165–194. https://doi.org/10.1023/A:1011945222010

Head, J. W., Wilson, L., Dickson, J., and Neukum, G. (2006). The Huygens–Hellas giant dike system on Mars: implications for Late Noachian–Early Hesperian volcanic resurfacing and climatic evolution. *Geology*, *34*(4), 285–288. https://doi.org/10.1130/G22163.1

Head, J. W., III, Hiesinger, H., Ivanov, M. A., Kreslavsky, M. A., Pratt, S., and Thomson, B. J. (1999). Possible ancient oceans on Mars: evidence from Mars orbiter laser altimeter data. *Science*, *286*(5447), 2134–2137. https://doi.org/10.1126/science.286.5447.2134

Head, J. W., III, Kreslavsky, M. A., and Pratt, S. (2002). Northern lowlands of Mars: evidence for widespread volcanic flooding and tectonic deformation in the Hesperian period. *J. Geophys. Res.: Planets*, *107*(E1), 5003. https://doi.org/10.1029/2000JE001445

Hemmi, R., and Miyamoto, H. (2017). Distribution, morphology, and morphometry of circular mounds in the elongated basin of northern Terra Sirenum, Mars. *Prog. Earth Planet. Sci.*, *4*(1), 26. https://doi.org/10.1186/s40645-017-0141-x

Hiesinger, H., and Head, J. W., III. (2000). Characteristics and origin of polygonal terrain in southern Utopia Planitia, Mars: results from Mars orbiter laser altimeter and Mars orbiter camera data. *J. Geophys. Res.: Planets*, *105*(E5), 11999–12022. https://doi.org/10.1029/1999JE001193

Huang, H., Liu, J. J., Wang, X., Chen, Y., Zhang, Q., Liu, D. W., Yan, W., and Ren, X. (2022). The analysis of cones within the Tianwen-1 landing area. *Remote Sens.*, *14*(11), 2590. https://doi.org/10.3390/rs14112590

Ivanov, B. A. (2001). Mars/moon cratering rate ratio estimates. *Space Sci. Rev.*, *96*(1–4), 87–104. https://doi.org/10.1023/A:1011941121102

Ivanov, M. A., Hiesinger, H., Erkeling, G., and Reiss, D. (2014). Mud volcanism and morphology of impact craters in Utopia Planitia on Mars: evidence for the ancient ocean. *Icarus*, *228*, 121–140. https://doi.org/10.1016/J.ICARUS.2013.09.018

Kopf, A. J. (2002). Significance of mud volcanism. *Rev. Geophys.*, *40*(2), 2. https://doi.org/10.1029/2000RG000093

Korteniemi, J., Raitala, J., Aittola, M., Ivanov, M. A., Kostama, V. P., Öhman, T., and Hiesinger, H. (2010). Dike indicators in the Hadriaca Patera–Promethei terra region, Mars. *Earth Planet. Sci. Lett.*, *294*(3–4), 466–478. https://doi.org/10.1016/J.EPSL.2009.06.038

Lanz, J. K., Wagner, R., Wolf, U., Kröchert, J., and Neukum, G. (2010). Rift zone volcanism and associated cinder cone field in Utopia Planitia, Mars. *J. Geophys. Res.: Planets*, *115*(E12), E12019. https://doi.org/10.1029/2010JE003578

Li, C. L., Zhang, R. Q., Yu, D. Y., Dong, G. L., Liu, J. J., Geng, Y., Sun, Z. Z., Yan, W., Ren, X., … Ouyang, Z. Y. (2021). China's Mars exploration mission and science investigation. *Space Sci. Rev.*, *217*(4), 57. https://doi.org/10.1007/S11214-021-00832-9

Liu, J. J., Li, C. L., Zhang, R. Q., Rao, W., Cui, X. F., Geng, Y., Jia, Y., Huang, H., Ren, X., … Zhang, H. B. (2022). Geomorphic contexts and science focus of the Zhurong landing site on Mars. *Nat. Astron.*, *6*(1), 65–71. https://doi.org/10.1038/s41550-021-01519-5

Liu, Y., Wu, X., Zhao, Y. Y. S., Pan, L., Wang, C., Liu, J., Zhao, Z. X., Zhou, X., Zhang, C. L., … Zou, Y. L. (2022). Zhurong reveals recent aqueous activities in

Utopia Planitia, Mars. *Sci. Adv.*, *8*(19), eabn8555. https://doi.org/10.1126/sciadv.abn8555

McGill, G. E. (1989). Buried topography of Utopia, Mars: persistence of a giant impact depression. *J. Geophys. Res.: Solid Earth*, *94*(B3), 2753–2759. https://doi.org/10.1029/JB094IB03P02753

McGowan, E. M. (2011). The Utopia/Isidis overlap: possible conduit for mud volcanism on Mars. *Icarus*, *212*(2), 622–628. https://doi.org/10.1016/j.icarus.2011.01.025

Michael, G. G., and Neukum, G. (2010). Planetary surface dating from crater size–frequency distribution measurements: partial resurfacing events and statistical age uncertainty. *Earth Planet. Sci. Lett.*, *294*(3–4), 223–229. https://doi.org/10.1016/J.EPSL.2009.12.041

Mills, M. M., McEwen, A. S., and Okubo, C. H. (2021). A preliminary regional geomorphologic map in Utopia Planitia of the Tianwen-1 Zhurong landing region. *Geophys. Res. Lett.*, *48*(18), e2021GL094629. https://doi.org/10.1029/2021GL094629

Mouginis-Mark, P. J. (1987). Water or ice in the Martian regolith? Clues from rampart craters seen at very high resolution. *Icarus*, *71*(2), 268–286. https://doi.org/10.1016/0019-1035(87)90152-7

Neukum, G., Ivanov, B. A., and Hartmann, W. K. (2001). Cratering records in the inner solar system in relation to the lunar reference system. *Space Sci. Rev.*, *96*(1–4), 55–86. https://doi.org/10.1023/A:1011989004263

Parker, T. J., Gorsline, D. S., Saunders, R. S., Pieri, D. C., and Schneeberger, D. M. (1993). Coastal geomorphology of the Martian northern plains. *J. Geophys. Res.: Planets*, *98*(E6), 11061–11078. https://doi.org/10.1029/93JE00618

Ruff, S. W., and Christensen, P. R. (2002). Bright and dark regions on Mars: particle size and mineralogical characteristics based on thermal emission spectrometer data. *J. Geophys. Res.: Planets*, *107*(E12), 5127. https://doi.org/10.1029/2001JE001580

Skinner, J. A. Jr., and Tanaka, K. L. (2007). Evidence for and implications of sedimentary diapirism and mud volcanism in the southern Utopia highland–lowland boundary plain, Mars. *Icarus*, *186*(1), 41–59. https://doi.org/10.1016/J.ICARUS.2006.08.013

Skinner, J. A. Jr., and Mazzini, A. (2009). Martian mud volcanism: terrestrial analogs and implications for formational scenarios. *Mar. Pet. Geol.*, *26*(9), 1866–1878. https://doi.org/10.1016/J.MARPETGEO.2009.02.006

Soare, R. J., Costard, F., Pearce, G. D., and Séjourné, A. (2012). A re-interpretation of the recent stratigraphical history of Utopia Planitia, Mars: implications for late-Amazonian periglacial and ice-rich terrain. *Planet. Space Sci.*, *60*(1), 131–139. https://doi.org/10.1016/J.PSS.2011.07.007

Soare, R. J., Horgan, B., Conway, S. J., Souness, C., and El-Maarry, M. R. (2015). Volcanic terrain and the possible periglacial formation of "excess ice" at the mid-latitudes of Utopia Planitia, Mars. *Earth Planet. Sci. Lett.*, *423*, 182–192. https://doi.org/10.1016/J.EPSL.2015.04.033

Solomon, S. C., and Head, J. W. (1980). Lunar Mascon Basins: lava filling, tectonics, and evolution of the lithosphere. *Rev. Geophys.*, *18*(1), 107–141. https://doi.org/10.1029/RG018I001P00107

Tanaka, K. L., Skinner, J. A. Jr., Hare, T. M., Joyal, T., and Wenker, A. (2003). Resurfacing history of the northern plains of Mars based on geologic mapping of Mars global surveyor data. *J. Geophys. Res.: Planets*, *108*(E4), 8043. https://doi.org/10.1029/2002JE001908

Tanaka, K. L., Skinner, J. A. Jr., Dohm, J. M., Irwin, R. P., III, Kolb, E. J., Fortezzo, C. M., Platz, T., Michael, G. G., and Hare, T. M. (2014). Geologic map of Mars (pp. 43). Reston: U. S. Geological Survey. https://doi.org/10.3133/sim3292

Thomson, B. J., and Head, J. W., III. (2001). Utopia Basin, Mars: characterization of topography and morphology and assessment of the origin and evolution of basin internal structure. *J. Geophys. Res.: Planets*, *106*(E10), 23209–23230. https://doi.org/10.1029/2000JE001355

Werner, S. C. (2009). The global Martian volcanic evolutionary history. *Icarus*, *201*(1), 44–68. https://doi.org/10.1016/J.ICARUS.2008.12.019

Wu, B., Dong, J., Wang, Y. R., Li, Z. J., Chen, Z. Y., Liu, W. C., Zhu, J. M., Chen, L., Li, Y., and Rao, W. (2021). Characterization of the candidate landing region for Tianwen-1—China's first mission to Mars. *Earth Space Sci.*, *8*(6), e2021EA001670. https://doi.org/10.1029/2021EA001670

Wu, X., Liu, Y., Zhang, C. L., Wu, Y. C., Zhang, F., Du, J., Liu, Z. H., Xing, Y., Xu, R., … Zou, Y. L. (2021). Geological characteristics of China's Tianwen-1 landing site at Utopia Planitia, Mars. *Icarus*, *370*, 114657. https://doi.org/10.1016/J.ICARUS.2021.114657

Yan, W., Liu, J. J., Ren, X., Li, C. L., Fu, Q., Wang, D., Dong, J. H., Zhang, X. X., Chen, W. L., … Wu, F. L. (2021). Detection capability verification and performance test for the high resolution imaging camera of China's Tianwen-1 mission. *Space Sci. Rev.*, *217*(6), 71. https://doi.org/10.1007/s11214-021-00844-5

Ye, B. L., Qian, Y. Q., Xiao, L., Michalski, J. R., Li, Y. L., Wu, B., and Qiao, L. (2021). Geomorphologic exploration targets at the Zhurong landing site in the southern Utopia Planitia of Mars. *Earth Planet. Sci. Lett.*, *576*, 117199. https://doi.org/10.1016/J.EPSL.2021.117199

Zhao, J. N., Xiao, Z. J., Huang, J., Head, J. W., Wang, J., Shi, Y. T., Wu, B., and Wang, L. (2021). Geological characteristics and targets of high scientific interest in the Zhurong landing region on Mars. *Geophys. Res. Lett.*, *48*(20), e2021GL094903. https://doi.org/10.1029/2021GL094903

Zimbelman, J. R., and Griffin, L. J. (2010). HiRISE images of yardangs and sinuous ridges in the lower member of the Medusae fossae formation, Mars. *Icarus*, *205*(1), 198–210. https://doi.org/10.1016/J.ICARUS.2009.04.003

Zuber, M. T., Solomon, S. C., Phillips, R. J., Smith, D. E., Tyler, G. L., Aharonson, O., Balmino, G., Banerdt, W. B., Head, J. W., … Zhong, S. J. (2000). Internal structure and early thermal evolution of Mars from Mars global surveyor topography and gravity. *Science*, *287*(5459), 1788–1793. https://doi.org/10.1126/SCIENCE.287.5459.1788